Supporting Information for "Comparing observations and parameterizations of ice-ocean drag through an annual cycle across the Beaufort Sea"

Samuel Brenner [1], Luc Rainville [1], Jim Thomson [1], Sylvia Cole [2], Craig Lee [1]

[1]Applied Physics Laboratory, University of Washington, Seattle, WA, USA

[2]Woods Hole Oceanographic Institution, Woods Hole, MA, USA

Contents of this file

Introduction This supporing information provides additional figures and tables and discusses the sensitivity of the results of the main study.

Text S1. *Sensitivity of results: geostrophic velocity*

The inclusion of the geostrophic velocity, $\boldsymbol{u}_g$ in eq. (3) arises from sea surface tilt in the sea ice momentum equation, and the assumption of geostrophic balance: $f\hat{k} \times \boldsymbol{u}_g = g\nabla\eta$. However, there is some ambiguity involved in defining a geostrophic velocity from ADCP-measured ocean velocity profiles. For the present study, $\boldsymbol{u}_g$ is based on the measured velocity averaged over some depth range, which has previously been found to be in good agreement with estimates of sea surface height from satellite altimetry on monthly timescales

(Armitage et al., 2017). Over a 12-year record in the Beaufort Sea, Armitage et al. (2017) found that the 5 m to 20 m depth range produced the best match between monthly averaged velocities and satellite altimetry estimates of geostrophic velocity. Other studies have used different depth ranges. For example, Randelhoff, Sundfjord, and Renner (2014) used an average velocity in the 17 m to 22 m depth range to represent the undisturbed ocean beneath sea ice and Cole et al. (2017) define a geostrophic reference velocity in reference to the depth of the mixed-layer. For consistency with Armitage et al. (2017), we define $\boldsymbol{u}_g$ as the average velocity from 5 m to 20 m depth low-pass filtered with a 2-day cut-off (to reflect that the geostrophic balance adjustment occurs over inertial timescales).

The values of $\boldsymbol{\tau}_{io}$ and C_{io} are fairly insensitive to the choice of averaging depth used to define the geostrophic velocity. Averaged through the full record, ice-ocean and atmosphere-ice stresses almost perfectly balance (table S1 and fig. S2). The Coriolis acceleration term is ∼3–4% of $\boldsymbol{\tau}_{io}$, but it largely cancelled by local acceleration and sea surface tilt. These results are generally consistent with those by Steele, Zhang, Rothrock, and Stern (1997), who also find a minimal contribution from Coriolis and tilt terms (their model neglected local acceleration). While different choices of the depth range used for averaging in the definition of $\boldsymbol{u}_g$ result in different relative contributions to the ice-ocean stress (table S1), these amount to differences in $\boldsymbol{\tau}_{io}$ on the order of ∼1–2% and aren't substantial enough to impact the calculated values of C_{io}.

Text S2. *Sensitivity of results: atmosphere-ice drag coefficient*

As the ice-ocean stress in free-drift conditions is largely set by the atmosphere-ice stress (table S1 and fig. S2), the values of $\boldsymbol{\tau}_{io}$ and consequently C_{io} will be sensitive to the atmosphere-ice stress. The atmospheric stress available from the ERA5 re-analysis prod-

uct represents the total effective stress $\boldsymbol{\tau}_{atm}$, which is the ice-concentration weighted average of atmosphere-ice and atmosphere-ocean stresses (reproduced from eq. 5b):

$$\boldsymbol{\tau}_{atm} = A\boldsymbol{\tau}_{ai} + (1 - A)\boldsymbol{\tau}_{ao}.$$

Thus, the re-analysis stress is not appropriate for predicting sea ice motion, which responds to the atmosphere-ice stress, $\boldsymbol{\tau}_{ai}$ (see eq. 2). Instead, the atmosphere-ice stress in this study is determined using the quadratic drag law (eq. 4b): $\boldsymbol{\tau}_{ai} = \rho_a C_{ai} \boldsymbol{u}_a |\boldsymbol{u}_a|$, with an atmosphere-ice drag coefficient C_{ai} (which accounts for the combined effects of both skin and form drag on the ice surface). In past studies of ice-ocean drag using a force balance approach, C_{ai} has been taken as a constant (T. W. Kim et al., 2017; Dewey, 2019), or may be an additional predicted result (which requires additional modelling; e.g., Heorton et al., 2019). The atmosphere-ice drag coefficient is expected to vary with bulk sea ice surface roughness similarly to the ice-ocean drag coefficient (Andreas, 2011; Lüpkes et al., 2012); however, a number of studies have described observed variations as functions of sea ice concentration, A (e.g., Andreas, Horst, et al., 2010; Andreas, Persson, et al., 2010; Lüpkes et al., 2012).

Here, we consider the sensitivity of the calculated ice-ocean drag values to the choice of parameterization of the atmosphere-ice drag coefficient, and describe the choice used in the main body of the study. Three schemes are considered: (1) the formulation from the European Centre for Medium-Range Weather Forecasts (ECMWF) model; (2) a constant drag coefficient; and (3) following a version of the parameterization by Lüpkes et al. (2012).

The ECMWF model (scheme 1) parameterizes the ice surface roughness as a function of ice concentration, A as (ECMWF, 2019):

$$z_{0M} = 10^{-3} \times \max\left\{1, \quad 0.93(1-A) + 6.05\exp[-17(A-0.5)^2]\right\}, \tag{S1}$$

which accounts for the combined effects of sea ice skin roughness and form drag. Then, the neutral drag coefficient $C_{ai} = [\kappa/\ln(z_{ref}/z_{0M})]^2$, with $z_{ref} = 10\,\mathrm{m}$.

The constant drag coefficient (scheme 2) is taken as $C_{ai} = 1.47 \times 10^{-3}$, based on a constant roughness length $z_{0M} = 2.3 \times 10^{-4}\,\mathrm{m}$ (appropriate for winter Arctic conditions; Andreas, Persson, et al., 2010).

The parameterization by Lüpkes et al. (2012) (scheme 3) forms the basis for the ice-ocean drag parameterization by Tsamados et al. (2014) and is based on ice geometry characteristics (similar to section 2.1); however, the authors provide a hierarchy of simplifications to the model based on empirical relationships found between ice morphology and concentration (also see Lüpkes et al., 2013). To construct C_{ai} only as a function of A based on Lüpkes et al. (2012) for the purpose of sensitivity testing, we use their eqs. 2 and 53–54 with h_f given by their eq. 25 and ignore the effects of melt ponds (consistent with Elvidge et al., 2016). Note that Lüpkes et al. (2012) parameterize a total equivalent neutral atmospheric drag coefficient as $C_{atm} = AC_{d,i} + (1-A)C_{ao} + C_{d,f}$, where $C_{d,i}$ is the skin drag on the ice surface and $C_{d,f}$ is the form drag (C_{ao} is the atmosphere-ocean drag). Since the form drag, $C_{d,f}$, acts only on the ice-covered area, the total atmosphere-ice drag coefficient (accounting for both skin and form drag) from the Lüpkes et al. (2012) formulations becomes $C_{ai} = C_{d,i} + C_{d,f}/A$.

The effective total atmospheric drag coefficient, C_{atm} (found as $C_{atm} = AC_{ai} + (1-A)C_{ao}$, where C_{ai} includes both skin as form drag contributions), has a similar character for both

the ECMWF scheme and the scheme by Lüpkes et al. (2012) (fig. S3a) while the constant drag scheme doesn't include the local maximum at intermediate sea ice concentrations (for fig. S3a, C_{ao} is set to a fixed value of 1.1×10^{-3} as an example, following Elvidge et al., 2016). However, these test cases give different forms of the atmosphere-ice drag coefficient, C_{ai}. The three schemes have somewhat similar values of C_{ai} at 100% ice concentration (values vary from 1.47×10^{-3} to 1.98×10^{-3}); however, at low concentrations, the value of C_{ai} can more than double depending on the choice of parametrization scheme (values vary from 1.47×10^{-3} to 3.91×10^{-3}; fig. S3b).

Despite the much higher C_{ai} during the fall season when using the Lüpkes et al. (2012) parameterization (compared to ECMWF; fig. S4a), the observed seasonal variations in the ice-ocean drag coefficient exist regardless of the C_{ai} scheme used (fig. S4b). The differences between the fall minimum and winter maximum C_{io} are slightly muted when using the Lüpkes et al. (2012) scheme for C_{ai}, but enhanced when using a constant atmosphere-ice drag coefficient (due to lower values of C_{ai} during the fall). While the seasonal patterns of C_{io} are robust across different C_{ai} parameterization schemes, the values of C_{io} are impacted by the choice of scheme for C_{ai}. Annual average values of C_{io} taken across all three moorings are 4.6×10^{-3} when using the ECMWF parameterization for C_{ai} (fig. 10), 4.1×10^{-3} for the Lüpkes et al. (2012) parameterization, and 3.3×10^{-3} for constant C_{ai}; these values directly reflect the proportional changes between C_{ai} calculated using the different parameterization schemes.

For the purpose of the main body of the text, $\boldsymbol{\tau}_{ai}$ is calculated with the quadratic drag law (eq. 4b), and uses the ECMWF (2019) method of atmosphere-ice drag calculation (C_{ai}), with a surface roughness given by eq. (1) that accounts for the effects of both skin

and form drag together. Thus, the chosen scheme is consistent with the ERA5 re-analysis product that is used for wind speed.

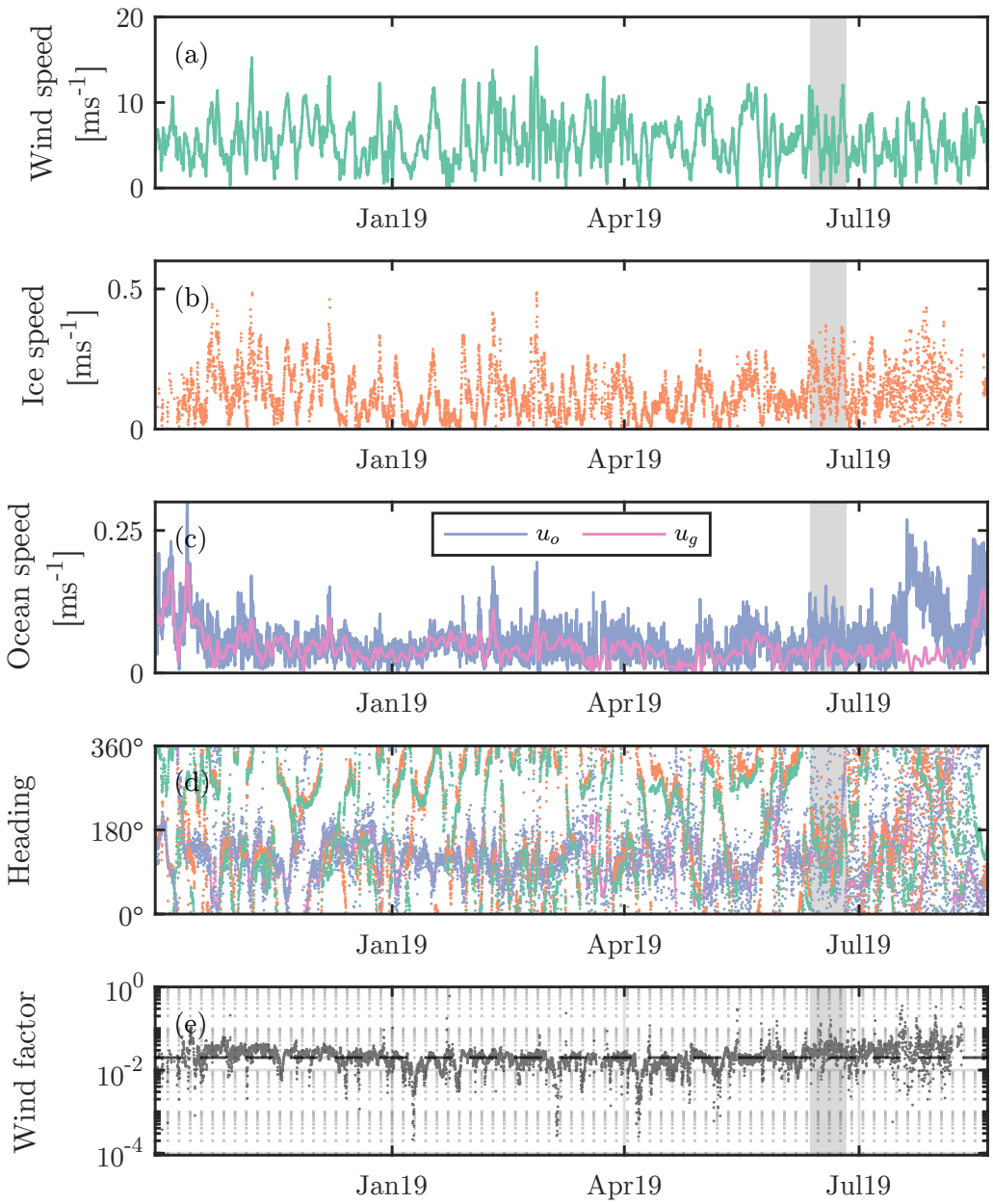

Figure S1. Hourly timeseries at SODA-B of (a) wind speed; (b) ice speed; (c) speed of ocean current at 10-m reference depth ($\boldsymbol{u}_o$) and geostrophic current ($\boldsymbol{u}_g$); (d) directions for each of the speeds in (a-c), coloured correspondingly (using a conventions of the direction each velocity vector is pointing towards measured clockwise from North); (e) wind factor ($|\boldsymbol{u}_i|/|\boldsymbol{u}_a|$). The shaded grey background shows the time period used in fig. S2.

Table S1. Annual median values of the stress components of each of the terms in the sea ice momentum balance (eq. 3) projected onto the direction of $\boldsymbol{\tau}_{io}$. Different rows for the sea surface tilt component, $\rho_o d_i f\hat{k} \times \boldsymbol{u}_g$, (labelled 1–4) correspond to different depth-ranges used for averaging in the definition of $\boldsymbol{u}_g$: (1) 5 m to 20 m, used for the main text; (2) 17 m to 22 m; (3) the full depth profile measured by the ADCP; and (4) rather an a depth-averaged velocity, $\boldsymbol{u}_g$ is defined by the velocity in the deepest ADCP bin.

	Projected stress [mPa]		
	SODA-A	SODA-B	SODA-C
$\boldsymbol{\tau}_{io}$	116.7	96.8	69.3
$\boldsymbol{\tau}_{ai}$	116.5	97.7	71.4
$-\rho_o d_i \frac{\partial \boldsymbol{u}_i}{\partial t}$	0.1	0.4	0.3
$-\rho_o d_i f\hat{k} \times \boldsymbol{u}_i$	-5.4	-2.7	-4.4
$^{(1)}$ $\rho_o d_i f\hat{k} \times \boldsymbol{u}_g$	5.0	1.5	1.5
$^{(2)}$ $\rho_o d_i f\hat{k} \times \boldsymbol{u}_g$	4.1	1.1	0.8
$^{(3)}$ $\rho_o d_i f\hat{k} \times \boldsymbol{u}_g$	3.6	0.9	1.3
$^{(4)}$ $\rho_o d_i f\hat{k} \times \boldsymbol{u}_g$	2.3	0.4	0.3

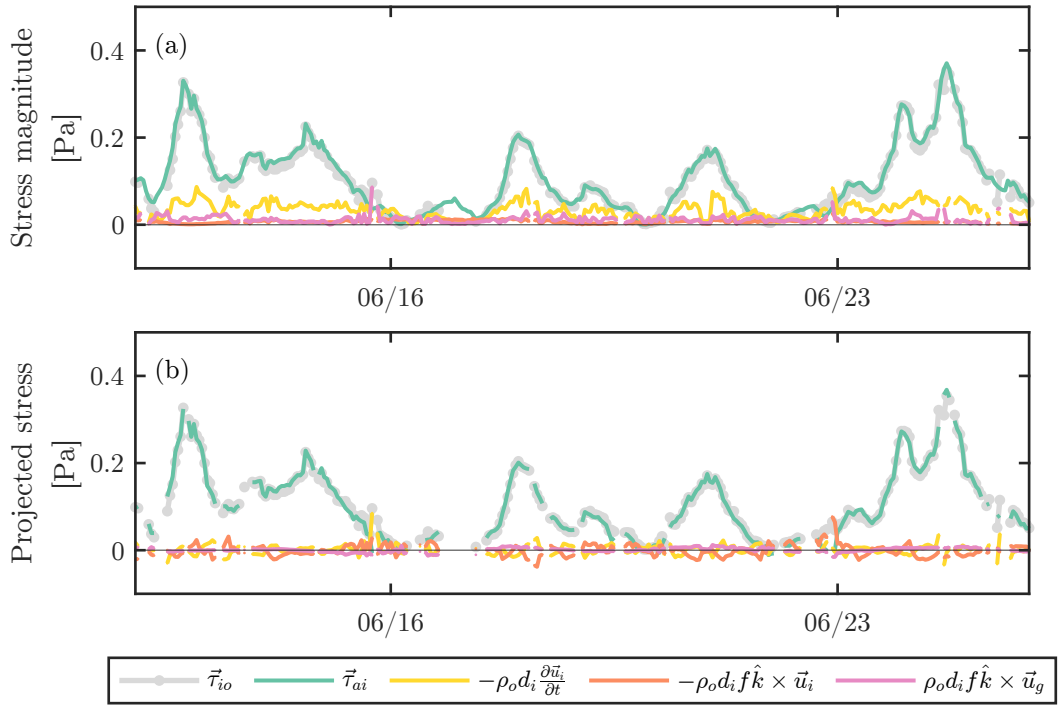

Figure S2. An example period from two week period in summer at SODA-B showing the size of different terms in the sea ice momentum balance (eq. 3): (a) magnitude of each stress component; (b) stress components projected onto the direction of $\boldsymbol{\tau}_{io}$. Missing values of $|\boldsymbol{\tau}_{io}|$ in (a) and of all stress components in (b) are due to the exclusion of $|\boldsymbol{\tau}_{io}|$ values when the wind factor is $< 2\%$.

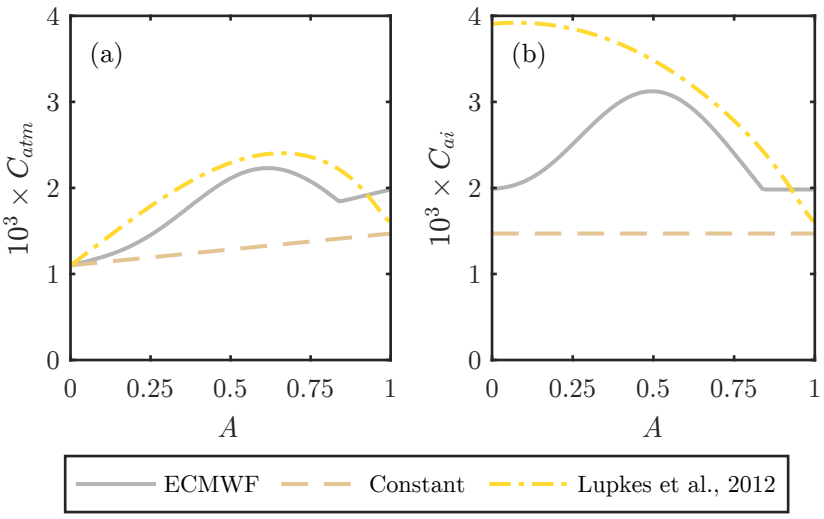

Figure S3. Parameterized drag coefficients as a function of sea ice concentration, A: (a) total effective atmospheric drag coefficient, C_{atm}; (b) atmosphere-ice drag coefficient, C_{ai}.

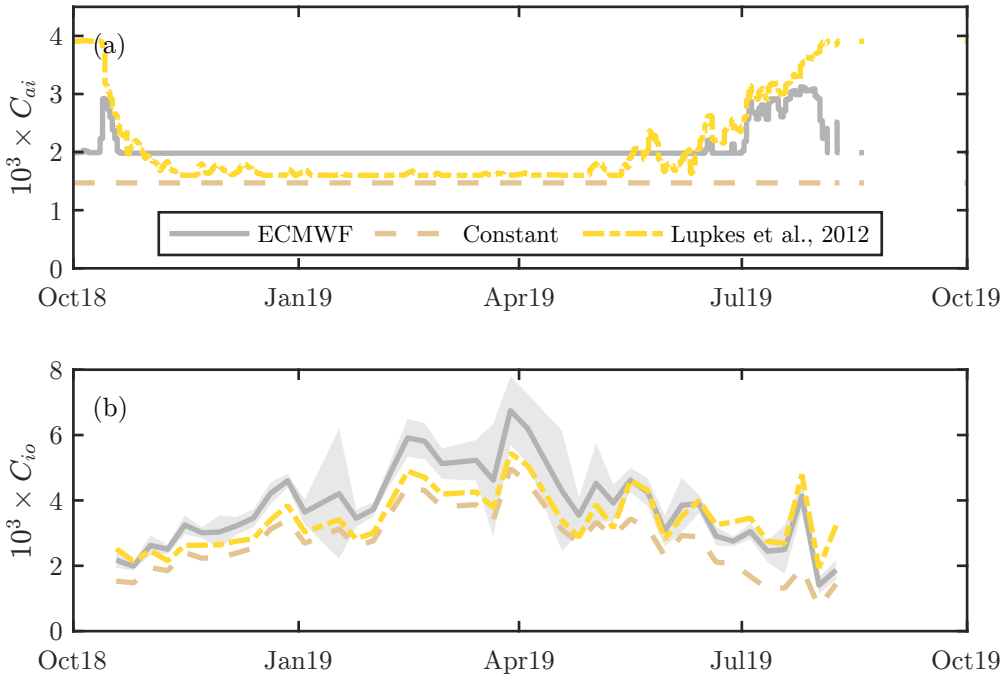

Figure S4. Timeseries at SODA-B of (a) atmosphere-ice drag coefficients, C_{ai}, calculated using different parameterization schemes, and (b) corresponding ice-ocean drag coefficients, C_{io}. The grey-shaded region in (b) shows the 95% uncertainty range associated with regression procedure to determine C_{io} when C_{ai} is calculated with the ECMWF scheme.